Tb^{3+} in $TbCo_3B_2$: A singlet ground state system studied by inelastic neutron scattering

Oleg Rivin*
Department of Physics, Nuclear Research Centre-Negev, P.O. Box 9001, Beer Sheva 84190, Israel and Department of Physics, Ben-Gurion University, P.O. Box 653, Beer Sheva 84105, Israel

Raymond Osborn
Materials Science Division, Argonne National Laboratory, 9700 South Cass Avenue, Argonne, Illinois 60439, USA

Alexander I. Kolesnikov
Intense Pulsed Neutron Source, Argonne National Laboratory, 9700 South Cass Avenue, Argonne, Illinois 60439, USA and Spallation Neutron Source, Oak Ridge National Laboratory, Oak Ridge, Tennessee 37831, USA

El'ad N. Caspi
Department of Physics, Nuclear Research Centre-Negev, P.O. Box 9001, Beer Sheva 84190, Israel

Hagai Shaked
Department of Physics, Ben-Gurion University, P.O. Box 653, Beer Sheva 84105, Israel
(Received 6 July 2008; published 19 November 2008)

The results of inelastic neutron scattering on the hexagonal compounds $TbCo_3B_2$ and $Tb_{0.75}Y_{0.25}Co_3B_2$, at several temperatures, are reported. The crystal-field level scheme of Tb^{3+} ions in the paramagnetic phase is determined. This scheme contains a nonmagnetic singlet (Γ_1) as the ground state. Inelastic neutron scattering at low temperature (10 K) leads to a different energy-level scheme, where the singlet ground state is ferromagnetic with $\langle J_x \rangle \neq 0$. This is a "self-induced" ferromagnetism on the Tb sublattice, resulting from the admixture of higher crystal-field levels into the singlet ground state by the exchange field. The resulting magnitudes of these ground state magnetic moments are $5.6(3)\mu_B$ and $3(1)\mu_B$ for $TbCo_3B_2$ and $Tb_{0.75}Y_{0.25}Co_3B_2$, respectively. These values are much smaller than the free ion value of $9\mu_B$ and are in agreement with previously observed values. Such large reductions are characteristic of the "self-induced" ferromagnetism. The temperature dependences of the magnetic moment, magnetic anisotropy, Tb sublattice dilution, and magnetic susceptibility are discussed.

DOI: 10.1103/PhysRevB.78.184424 PACS number(s): 75.25.+z, 75.30.Gw, 75.47.Np, 75.50.Gg

I. INTRODUCTION

Materials of the $R_{n+1}Co_{3n+5}B_{2n}$ (R=lanthanides; $n=1,2,3,\infty$) family are of hexagonal symmetry ($P6/mmm$ space group[1]) and are derived from the RCo_5 ($n=0$) by partial substitution of B for Co in one of the two Co sites [2c (Ref. 1)] until a complete substitution is achieved on that site for RCo_3B_2 ($n=\infty$).[2] The hexagonal lattice parameters of $TbCo_3B_2$ are $a\sim5$ Å and $c\sim3$ Å.[3] Upon cooling, $TbCo_3B_2$ undergoes a ferromagnetic ordering of the Co sublattice at $T_{Co}\sim170$ K, with $\mu_{Co}\sim0.1\mu_B$ along the hexagonal axis.[3] This ordered Co moment induces a moment of $\sim0.5(2)\mu_B$ on the Tb ion.[3] Upon further cooling, a ferromagnetic ordering of the Tb sublattice takes place at $T_{Tb}\sim30$ K for $TbCo_3B_2$ ($T_{Tb}\equiv T_{SRT}$ in Ref. 3), with $\mu_{Tb}=5.2(1)\mu_B$ approximately perpendicular to the hexagonal axis. Below T_{Tb}, μ_{Co} reorients toward the hexagonal plane, into a direction opposite to μ_{Tb}, making the system a collinear ferrimagnetic.[3] The observed value of $5.2(1)\mu_B$ determined using neutron powder diffraction (NPD) and magnetization measurements exhibits an unexplained reduction compared to the Tb^{3+} free ion value of $9\mu_B$[3]. Moreover, in a recent NPD study of the Y diluted Tb sublattice, $Tb_{0.75}Y_{0.25}Co_3B_2$, in which the Tb sublattice orders at $T_{Tb}\sim17$ K, a considerably lower value of $1.7(2)\mu_B$ was observed for the Tb^{3+} ion.[4]

A complete orbital quenching of the magnetic moment of the Tb^{3+} free ion ($^7F_6$) will reduce the magnetic moment to $6\mu_B$. Hence, orbital quenching (which is quite uncommon with lanthanides) could not be used to explain these low values of the observed μ_{Tb}. It was previously shown[5,6] that the combined action of the crystalline electric field (CEF) and the exchange field in the R sublattice causes a reduction in the value of the magnetic moment. In this paper, we therefore investigate these CEF and exchange interactions in detail by the inelastic neutron-scattering (INS) technique.

A brief description of the INS experiment and its results is provided in Secs. II, III, and IV A. In Secs. IV B and IV C, we determine the energy levels and their wave functions by fitting the $T>T_{Tb}$ and the $T<T_{Tb}$ results to the CEF (Sec. IV B) and the CEF-magnetic (Sec. IV C) Hamiltonians, respectively. In Sec. IV D, we deduce the ground state ordered magnetic moments for the $TbCo_3B_2$ and the $Tb_{0.75}Y_{0.25}Co_3B_2$ data. These results, their temperature dependencies, magnetic anisotropy, and magnetic susceptibility are discussed in Sec. V.

II. EXPERIMENTAL DETAILS

Polycrystalline $TbCo_3B_2$, yttrium diluted $Tb_{0.75}Y_{0.25}Co_3B_2$, and nonmagnetic YCo_3B_2 were prepared

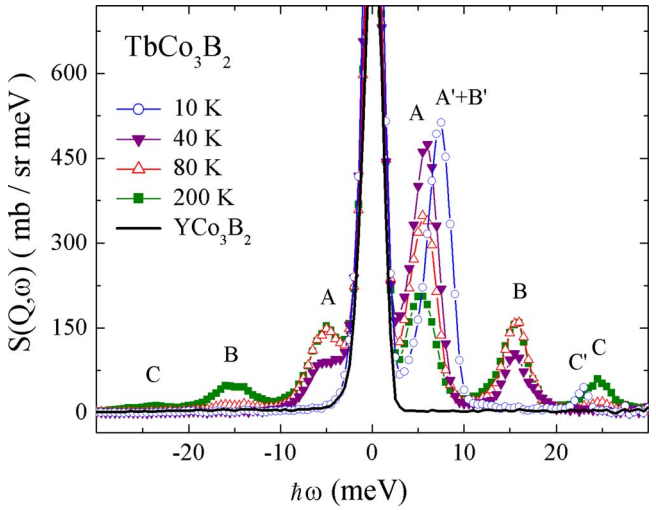

FIG. 1. (Color online) Response function, $S(Q,\omega)$, vs neutron energy loss, $\hbar\omega$, for $TbCo_3B_2$, with incident energy of E_0 =35 meV, at four temperatures (the lines are guides for the eyes). All nonelastic INS lines are of magnetic origin, as was verified using measurement of the nonmagnetic analog YCo_3B_2 at 200 K. These signals are noted by A, B, and C above magnetic ordering and A′, B′, and C′ below magnetic ordering. The measured momenta and angle ranges are $Q \in (2.01, 3.88)$ Å^{-1} and $2\theta \in (12°, 68.4°)$, respectively. Errors are smaller than the symbol size.

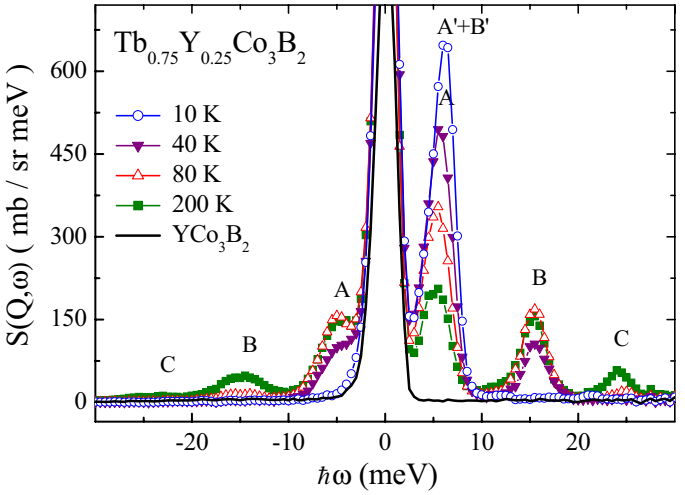

FIG. 2. (Color online) Response function, $S(Q,\omega)$, vs neutron energy loss, $\hbar\omega$, for $Tb_{0.75}Y_{0.25}Co_3B_2$, with incident energy of E_0 =35 meV, at four temperatures (the lines are guides for the eyes). All nonelastic INS lines are of magnetic origin, as was verified using measurement of the nonmagnetic analog YCo_3B_2 at 200 K. These signals are noted by A, B, and C above magnetic ordering and A′, B′, and C′ below magnetic ordering. The measured momenta and angle ranges are $Q \in (2.01, 3.88)$ Å^{-1} and $2\theta \in (12°, 68.4°)$, respectively. Errors are smaller than the symbol size.

in an arc melting furnace. The B used in all samples is ^{11}B in order to reduce thermal-neutron absorption. All samples used in the present work were prepared, characterized, and identified in previous work by various methods.[3,4,7] INS experiments were conducted on the time-of-flight low resolution medium energy chopper spectrometer (LRMECS) (Ref. 8) at the Intense Pulsed Neutron Source (IPNS) at the Argonne National Laboratory (ANL) at two incident neutron energies (35 and 60 meV) and four different sample temperatures (200, 80, 40, and 10 K). The experimental results were corrected using an instrumental background measured at the same experimental conditions and put on an absolute scale using vanadium measurements. The inelastic nonmagnetic background was determined by measuring the nonmagnetic analog, YCo_3B_2, at 200 K under identical experimental conditions. The polycrystalline flat sample was pressed from both sides by two aluminum sheets with area of $\sim 5 \times 10$ cm^2, to an ~ 3 mm thickness, in order to reduce absorption. Aluminum was used to reduce background scattering. The net weights of the $TbCo_3B_2$, $Tb_{0.75}Y_{0.25}Co_3B_2$, and YCo_3B_2 samples were 13.48, 16.68, and 10.01 g, respectively.

III. RESULTS

INS data above (T=40, 80, and 200 K) and below (T =10 K) T_{Tb} are presented for $TbCo_3B_2$ and for $Tb_{0.75}Y_{0.25}Co_3B_2$ in Figs. 1 and 2, respectively. These data were collected using an incident energy of E_0=35 meV. An additional incident energy of E_0=60 meV was used (not shown) to verify that no INS lines appear at higher transfer energies. The observed transfer of energy from the neutron to the sample, $\hbar\omega$, is determined from the time difference in the detector array between inelastically and elastically scattered neutrons. The response function,[9] $S(Q,\omega)$ [Eq. (1)], is proportional to the (partial) differential cross section for magnetic INS (disregarding the elastic peak),

$$\frac{\partial^2\sigma}{\partial\Omega\,\partial\omega} = \frac{k'}{k} S(Q,\omega), \tag{1}$$

where $\hbar k$ and $\hbar k'$ are, respectively, the incoming and outgoing (after interaction with the sample) momenta of the neutron. These response functions were normalized to zero-momentum transfer, Q=0, using the magnetic form factor of the Tb^{3+} ion[10] and calibrated on an absolute scale using vanadium measurement.

The inelastic nonmagnetic background (e.g., phonons) should be observed in the measurement of the nonmagnetic analog, YCo_3B_2, in our data at 200 K (Figs. 1 and 2). This background is undetectable. Furthermore, the decay of the magnetic INS lines with momentum transfer, Q, matches that of the Tb^{3+} "form factor."[9] This is expected in crystal-field transition in a paramagnetic state for temperatures above the Tb ordering temperature. Thus, we assume that all INS lines are of magnetic origin. For $T > T_{Tb}$, three crystal-field transitions are observed (A, B, and C in Figs. 1 and 2).

The validity of the experiment and temperature readings was confirmed by the "detailed balance" relation [Eq. (2)], where k_B is Boltzmann's constant and T is the temperature in kelvin,[9]

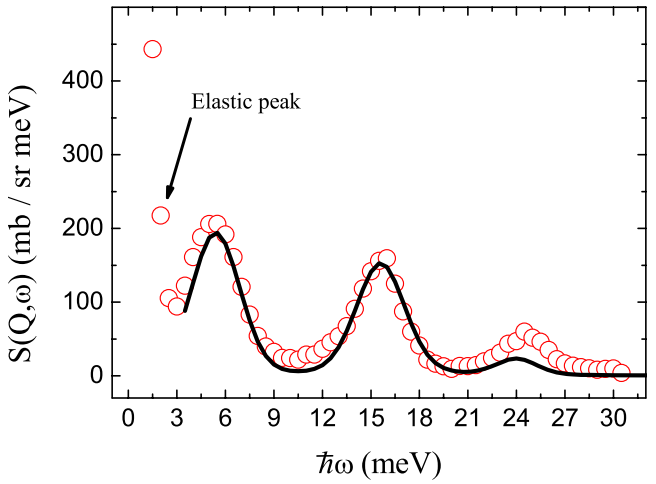

FIG. 3. (Color online) INS of $TbCo_3B_2$ at $T=200$ K. Observed data are represented by open circles. Calculated data were obtained using the least-squares fit algorithm (solid line; see text). The line shape was calculated (semiempirically) using a convolution of Gaussian and Lorentzian. Experimental errors are smaller than symbol size.

$$S(Q,-\omega) = e^{-\hbar\omega/k_B T} S(Q,\omega). \quad (2)$$

Equation (2) states that the ratio between the response functions describing an inelastic-scattering event, in which energy of $\hbar\omega$ is transferred from the neutron to the sample and vice versa, is determined only by the probability for thermal occupation of an excited state in the sample, given by Boltzmann's statistics. The inelastic lines at $T=10$ K (i.e., A′, B′, and C′) are shifted in energy transfer from their position at higher temperatures, suggesting a change in the energy-level scheme.

IV. ANALYSIS

A. INS of Tb^{3+} in crystalline environment

The CEF interaction removes the degeneracy of the ground multiplet $^7F_6$ in the free Tb^{3+} ion. The discrete levels generated by the CEF are experimentally determined by the INS technique. In this experiment, the sample is irradiated by a monochromatic neutron beam. These neutrons interact magnetically with the moment of the electrons of the $4f$ shell, causing transitions between the energy levels within the ground multiplet. The (inelastically) scattered neutrons are then analyzed, according to their energies. This analysis yields the energy transferred to and from the neutron; hence, the intramultiplet levels (eigenvalues) separations. The next multiplet (in the free Tb^{3+} ion), $^7F_5$, is 253 meV above the ground multiplet,[11] so the entire level splitting induced by the CEF and exchange interactions is considerably smaller than intermultiplet splitting. Thus, we neglect higher lying multiplets in the present analysis. The intensity of the scattered neutrons, at each energy transfer, depends on the transition rate between the levels. The transition rate is governed by the cross section for magnetic scattering by an isolated ion[12] and is used to find the wave functions (eigenstates) of each level. The small exchange generated by the Co-Co ordering below $T\sim 170$ K was neglected from the model.[4]

TABLE I. Refined CEF parameters (in meV) obtained by the least-squares fitting procedure simultaneously to all temperatures above T_{Tb}. Numbers in parentheses are the standard deviation of the last significant figure.

χ^2	B_2^0	B_4^0	B_6^0	B_6^6
9.0	1.40(3)	$-6(1)\times10^{-4}$	$3.1(5)\times10^{-6}$	$4.0(4)\times10^{-5}$

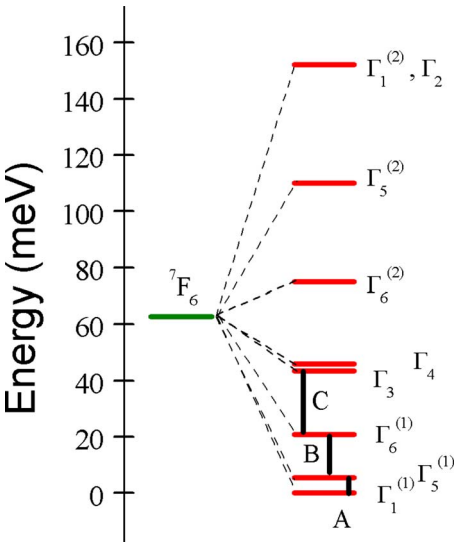

FIG. 4. (Color online) Energy level scheme of the eigenvalues of CEF Hamiltonian [Eq. (3)], $T>T_{Tb}$, for the Tb^{3+} ion in both samples. The levels are labeled by their eigenstate symmetries (Ref. 13). The solid lines, noted by A, B, and C, represent experimentally observed transitions using INS. The zero of the energy scale corresponds to the ground state at $T>T_{Tb}$.

B. CEF Hamiltonian

For $T>T_{Tb}$ ($T=40$, 80, and 200 K), the CEF Hamiltonian for hexagonal symmetry is given by[13,14]

TABLE II. Eigenvalues (Fig. 4) and eigenstates calculated (see text) by applying the CEF Hamiltonian [Eq. (1)] to the observed ($T>T_{Tb}$) data. The uncertainty in each eigenvalue is estimated as 2% using the relative shift between peak centers between the calculated (refined) and observed INS data (Fig. 3). Uncertainty in the energetic position of the entire multiplet (Fig. 4) is estimated as 20% using the errors in the refined parameters (Table I).

	Eigenvalue (meV)	Symmetry	Eigenstate
E_0	0	$\Gamma_1^{(1)}$	$-1\times\|0\rangle$
			$1\times\|+1\rangle$
E_1	6(1)	$\Gamma_5^{(1)}$	$1\times\|-1\rangle$
			$1\times\|+2\rangle$
E_2	21(1)	$\Gamma_6^{(1)}$	$1\times\|-2\rangle$
E_3	44(2)	Γ_3	$0.7\times\|+3\rangle-0.7\times\|-3\rangle$

$$H_{\mathrm{CEF}} = B_2^0 O_2^0 + B_4^0 O_4^0 + B_6^0 O_6^0 + B_6^6 O_6^6, \quad (3)$$

where the B_l^m and O_l^m are CEF parameters and Stevens operators, respectively.[15] The first three terms in the Hamiltonian [Eq. (3)] are diagonal in the J_z state basis.[14] The nondiagonal term, $B_6^6 O_6^6$, mixes the pure J_z states so that the eigenstates of the Hamiltonian [Eq. (3)] contain admixtures of different values of J_z. In the experimental resolution limit, the positions of the lines do not change with neither temperature nor with Y dilution. Thus, we assume that the CEF parameters are equal for the two samples and are temperature independent.

The least-squares (LS) fitting program, FRILLS,[12] was used to simultaneously fit data taken at the three temperatures ($T > T_{\mathrm{Tb}}$) of $TbCo_3B_2$. The procedure is based on the cross section for magnetic scattering[12] and the Hamiltonian [Eq. (3)]. A typical quality of the fit is illustrated in Fig. 3 for $T = 200$ K as an example. The discrepancy emerges mainly from low statistical weight given by the LS algorithm to the low intensity peak and poor line-shape description. The refined CEF parameters are summarized in Table I.

The energy eigenvalues thus obtained for both samples lead to the level scheme presented in Fig. 4. The eigenvalues and eigenstates for the Tb^{3+} ion for both samples are summarized in Table II. The allowed symmetries of the eigenstates of the Tb^{3+} ion in a CEF with $6/mmm$ symmetry are[13] $2\Gamma_1+\Gamma_2+\Gamma_3+\Gamma_4+2\Gamma_5+2\Gamma_6$. The Γ_i labels were assigned to the energy levels (Fig. 4) according to the transformation properties of their eigenstates (Table II). The small exchange generated by the Co-Co ordering below $T \sim 170$ K was neglected from the model.[4]

C. CEF-magnetic Hamiltonian

Below the Tb ordering temperature, T_{Tb}, an exchange term, perpendicular[4] to the unique hexagonal axis (i.e., J_x), is added to the CEF Hamiltonian,

$$H = H_{\mathrm{CEF}} + g\mu_B H_m J_x, \quad (4)$$

where $g = 3/2$ is the gyromagnetic ratio of the free Tb^{3+} ($^7F_6$) ion and H_m is the exchange field within the Weiss field approximation.[5] The cross section, $\partial^2\sigma_{\mathrm{iso}}/\partial\Omega\partial\omega$, is not valid in this case because the Tb moments are correlated due to their exchange. Thus, a simple fitting procedure is employed (position only of the INS lines) for the exchange field, H_m, using the $T > T_{\mathrm{Tb}}$ values of the CEF parameters (Table I). The values of $\mu_B H_m$, thus refined in $TbCo_3B_2$ and $Tb_{0.75}Y_{0.25}Co_3B_2$, are given in Table III.

TABLE III. Refined values of the exchange field, $\mu_B H_m$ (in meV), for $TbCo_3B_2$ and $Tb_{0.75}Y_{0.25}Co_3B_2$. Numbers in parentheses are the standard deviation of the last significant figure.

$TbCo_3B_2$	$Tb_{0.75}Y_{0.25}Co_3B_2$
0.50(5)	0.2(1)

Similarly to Sec. IV A, an energy-level scheme of the eigenvalues for $TbCo_3B_2$ is presented in Fig. 5 and summarized in Table IV. The allowed symmetries of the eigenstates of the Tb^{3+} ion in the magnetic Hamiltonian [Eq. (4)] with $2/m$ symmetry are[13] $7\Gamma_1+6\Gamma_2$ (Γ_1 and Γ_2 are all even). The Γ_i labels were assigned to the energy levels (Fig. 5) according to the transformation properties of their eigenstates (Table IV). The small exchange generated by the Co-Co ordering below $T \sim 170$ K was neglected from the model.[4]

D. Magnetic moment

The magnitudes of the ordered Tb magnetic moments ($T < T_{\mathrm{Tb}}$) for $TbCo_3B_2$ and $Tb_{0.75}Y_{0.25}Co_3B_2$ were calculated [Eq. (5)] using their ground state eigenstates (Table V) and are given in Table V,

$$\mu = g\mu_B \langle \Gamma_1^{(1)} | J_x | \Gamma_1^{(1)} \rangle. \quad (5)$$

Contribution from higher lying levels is neglected in Eq. (5) due to very low thermal occupation for temperatures below Tb ordering.

V. DISCUSSION AND CONCLUSIONS

For $T > T_{\mathrm{Tb}}$, the CEF interaction generates a singlet ground state ($\Gamma_1^{(1)} = |0\rangle$), for which quantum coupling between the ground and excited states generates regions of fluctuating ordered Tb^{3+} magnetic moment. This "order" is accompanied by fluctuating exchange fields. As the tempera-

TABLE IV. Eigenvalues (Fig. 5) and eigenstates calculated (see text) by applying the magnetic Hamiltonian [Eq. (4)] to the observed ($T < T_{\mathrm{Tb}}$) data and using the CEF values obtained for $T > T_{\mathrm{Tb}}$ in Sec. IV A. The uncertainties in the eigenvalues were calculated using the errors in the refined parameters (Tables I and III).

	Eigenvalue	Symmetry	Eigenstate
E_0	−1.5(1)	$\Gamma_1^{(1)}$	$0.9\times\|0\rangle - 0.3\times\|+1\rangle - 0.3\times\|-1\rangle$
E_1	6(1)	$\Gamma_2^{(1)}$	$0.7\times\|+1\rangle - 0.7\times\|-1\rangle - 0.1\times\|+2\rangle + 0.1\times\|-2\rangle$
E_2	8(1)	$\Gamma_1^{(2)}$	$0.5\times\|0\rangle + 0.6\times\|+1\rangle + 0.6\times\|-1\rangle - 0.1\times\|+2\rangle - 0.1\times\|-2\rangle$
E_3	20(10)	$\Gamma_2^{(2)}$	$0.1\times\|+1\rangle - 0.1\times\|-1\rangle + 0.7\times\|+2\rangle - 0.7\times\|-2\rangle - 0.1\times\|+3\rangle + 0.1\times\|-3\rangle$
E_4	20(10)	$\Gamma_1^{(3)}$	$-0.1\times\|+1\rangle - 0.1\times\|-1\rangle - 0.7\times\|+2\rangle - 0.7\times\|-2\rangle + 0.1\times\|+3\rangle + 0.1\times\|-3\rangle$

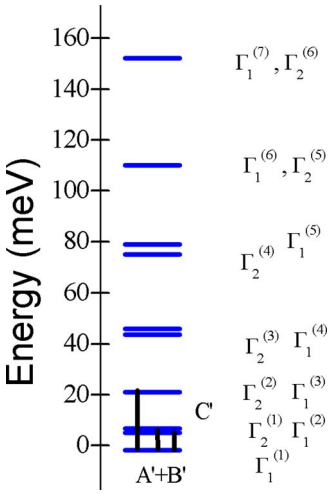

FIG. 5. (Color online) Energy level scheme of the eigenvalues of the magnetic Hamiltonian [Eq. (4)], $T<T_{\mathrm{Tb}}$, for the Tb^{3+} ion in $TbCo_3B_2$. The levels are labeled by their eigenstate symmetries (Ref. 13). The solid lines (vertical short), noted by A′, B′, and C′, represent experimentally observed transitions (Fig. 1). The zero of the energy scale corresponds to the ground state at $T>T_{\mathrm{Tb}}$.

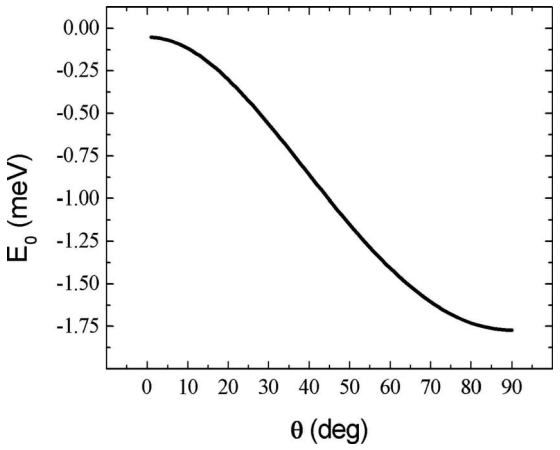

FIG. 6. Calculated magnetic anisotropy energy of the ground state of the magnetic Hamiltonian for $TbCo_3B_2$. The zero of the energy scale corresponds to the ground state at $T>T_{\mathrm{Tb}}$.

ture is lowered, regions of ions become more susceptible to these fields. At the critical temperature, T_{Tb}, the mean moment is large enough to sustain a mean exchange field, H_m (Weiss field), and long-range order sets in. This is a sort of a "bootstrap" process. Due to the anisotropy in the CEF interaction (see below), an exchange field perpendicular to the hexagonal axis results in a more stable ground state (Fig. 6). These CEF and exchange interactions generate a nondiagonal Hamiltonian [Eq. (4)], which admixes higher lying states into the ground state. The relative strength between the exchange interaction and the CEF determines the magnetic state of such "self-induced" moment systems.

Using the CEF-magnetic Hamiltonian [Eq. (4)], we are able to account for the anisotropy in our system, which causes the Tb magnetic moment to lie in the hexagonal plane. The magnitude of the exchange field, H_m, does not depend, to a first approximation, on the magnetic-moment direction. Hence, using Eq. (4) with J_x replaced by $J_x \sin^2\theta + J_z \cos^2\theta$, calculating the ground state energy, E_0, as a function of θ, clearly shows (Fig. 6) the magnetic anisotropy energy.

The magnetic susceptibility, χ, of a singlet ground state system leads to the Van-Vleck model for a two level system.[16] Adding an exchange field, H_m, changes the inverse susceptibility $1/\chi$ to $1/\chi - H_m/\mu$; hence,[5]

$$\frac{1}{\chi} = \frac{\Delta}{4g^2\mu_B^2} \frac{1}{|\langle \Gamma_1^{(1)}|J_x|\Gamma_5^{(1)}\rangle|^2} \frac{1}{\tanh\left(\frac{\Delta}{2k_BT}\right)} - \frac{H_m}{\mu}, \qquad (6)$$

where $\Delta \equiv E_1 - E_0$ is the separation energy between the ground and the first-excited state and μ is defined in Eq. (5). The Van-Vleck term in Eq. (6) was multiplied by a factor of 2 because there are two equivalent excited states above the singlet ground state (Fig. 4 and Table II). Solving the equation $1/\chi=0$ yields ordering temperatures of $T_{\mathrm{Coop}}=41(7)$ and 25(10) K for $TbCo_3B_2$ and $Tb_{0.75}Y_{0.25}Co_3B_2$, respectively. These values roughly agree with the observed[3,4] $T_{\mathrm{Tb}}=30(3)$ and 17(2) K using magnetization measurements.

There is a critical value, $\mu_B H_m^{(c)}=0.14(1)$ meV, for the exchange field,[16] below which there is no solution to the equation $1/\chi=0$ and thus magnetic ordering for Tb^{3+} ions is not possible for $\mu_B H_m^{(c)}<0.14(1)$ meV. This critical value is determined by the CEF interaction and therefore is approximately constant for all compounds $Tb_{1-x}Y_xCo_3B_2$. Assuming that the decrease in H_m is linear with Y concentration, we conclude that Tb ordering is not possible in $Tb_{1-x}Y_xCo_3B_2$ for $x>0.3(1)$ according to our model.

The observed magnetic moments in the present experiment for $x=0$ and 25 are (Table V) $5.6(3)\mu_B$ and $3(1)\mu_B$, respectively. These values agree within experimental uncertainty with respective values of $5.2(1)\mu_B$ and $1.7(2)\mu_B$, previously observed in powder-diffraction experiments.[3,4] The large uncertainty reported in the magnetic moment for $Tb_{0.75}Y_{0.25}Co_3B_2$ in this work results from the difficulty of

TABLE V. Magnetic moments in $TbCo_3B_2$ and $Tb_{0.75}Y_{0.25}Co_3B_2$, calculated using the admixed ground state wave function [Eq. (5)], due to exchange field H_m (Table III).

	H_m (meV)	Magnetic ground state	μ_x (μ_B)
$TbCo_3B_2$	0.50(5)	$+0.9\times\|0\rangle - 0.3\times\|+1\rangle - 0.3\times\|-1\rangle$	5.6(3)
$Tb_{0.75}Y_{0.25}Co_3B_2$	0.2(1)	$-0.95\times\|0\rangle + 0.2\times\|+1\rangle + 0.2\times\|-1\rangle$	3(1)

measuring the small exchange interaction compared to the CEF potential. It is worth noting that the relatively high angular momentum ($J=6$) of the Tb^{3+} ion, perpendicular to the c axis, generates high transition probability for magnetic scattering,[12] making this compound a very good candidate for an INS study.

ACKNOWLEDGMENTS

This work is based on an experiment No. 5385, performed at the Intense Pulsed Neutron Source, Argonne National Laboratory, Argonne, IL, USA. ANL is managed by UChicago Argonne, LLC, for the U.S. Department of Energy under Contract No. DE-AC02-06CH11357. One of us (A.I.K.) wishes to acknowledge ORNL/SNS which is managed by UT-Battelle, LLC, for the U.S. Department of Energy under Contract No. DE-AC05-00OR22725. The authors wish to thank Lynnete Jirik and Kristina Verdal for their assistance in conducting the experiment.

*Corresponding author. FAX: +972-8-6567878; olegr@nrcn.org.il

[1] *International Tables for Crystallography*, Space-Group Symmetry Vol. 1, edited by Th. Hahn (Kluwer, Dordercht, 1995).
[2] E. A. Nesbitt and J. H. Wernick, *Rare Earth Permanent Magnets* (Academic Press, New York, 1973).
[3] M. Dubman, E. N. Caspi, H. Ettedgui, L. Keller, M. Melamud, and H. Shaked, Phys. Rev. B **72**, 024446 (2005).
[4] E. Wolfson, E. N. Caspi, M. Avdeev, and H. Shaked, J. Magn. Magn. Mater. **320**, L97 (2008).
[5] B. Bleaney, Proc. R. Soc. London, Ser. A **276**, 19 (1963).
[6] G. T. Trammell, Phys. Rev. **131**, 932 (1963).
[7] O. Sigalov, A. I. Shames, E. N. Caspi, M. Dubman, H. Ettedgui, S. D. Goren, and H. Shaked, J. Appl. Phys. **98**, 074105 (2005).
[8] P. E. Sokol, K. Skold, D. L. Price, and R. Kleb, Phys. Rev. B **54**, 909 (1985). See also http://www.pns.anl.gov/instruments/lrmees/
[9] S. W. Lovesey, *Theory of Neutron Scattering from Condensed Matter*, (Oxford University Press, Oxford, 1987).
[10] G. H. Lander, T. O. Brun, J. P. Desclaux, and A. J. Freeman, Phys. Rev. B **8**, 3237 (1973).
[11] W. C. Martin, R. Zalubus, and L. Hagan, *Atomic Energy Levels of the Rare Earth Elements*, Natl. Bur. Stand. (U.S.) Circ. No. 60 (U.S. GPO, Washington, D.C., 1978), p. 259.
[12] S. Rosenkranz, M. Medarde, F. Fauth, J. Mesot, M. Zolliker, A. Furrer, U. Staub, P. Lacorre, R. Osborn, R. S. Eccleston, and V. Trounov, Phys. Rev. B **60**, 14857 (1999).
[13] M. Hammermesh, *Group Theory* (Addison-Wesley, Reading, MA, 1962); G. F. Koster, J. O. Dimmock, R. G. Wheeler, and H. Statz, *Properties of the Thirty-Two Point-Groups* (MIT, Cambridge, 1963).
[14] E. Bauer and M. Rotter, Proceedings of the CMA Euroschool, Ljubljana, Slovenia, 2007 http://euroschoolcma.ijs.si/CMAlectures07/bauer/CEFlecturebauer.pdf.
[15] K. W. H. Stevens, Proc. Phys. Soc., London, Sect. A **65**, 209 (1952).
[16] B. R. Cooper and O. Vogt, J. Phys. (Paris), Colloq. C1 **32**, 958 (1971).